



HAL
open science

Planar crack identification in 3D linear elasticity by the Reciprocity Gap method

Renaud Ferrier, Mohamed Larbi Kadri, Pierre Gosselet

► **To cite this version:**

Renaud Ferrier, Mohamed Larbi Kadri, Pierre Gosselet. Planar crack identification in 3D linear elasticity by the Reciprocity Gap method. *Computer Methods in Applied Mechanics and Engineering*, 2019, 355, pp.193-215. 10.1016/j.cma.2019.06.017 . hal-01907336

HAL Id: hal-01907336

<https://hal.science/hal-01907336>

Submitted on 29 Oct 2018

HAL is a multi-disciplinary open access archive for the deposit and dissemination of scientific research documents, whether they are published or not. The documents may come from teaching and research institutions in France or abroad, or from public or private research centers.

L'archive ouverte pluridisciplinaire **HAL**, est destinée au dépôt et à la diffusion de documents scientifiques de niveau recherche, publiés ou non, émanant des établissements d'enseignement et de recherche français ou étrangers, des laboratoires publics ou privés.

Planar crack identification in 3D linear elasticity by the Reciprocity Gap method

R. Ferrier, M. Kadri, P. Gosselet

October 16, 2018

Abstract

We study the reciprocity gap method [4] for the identification of planar cracks in the framework of three dimensional linear elasticity. In order to achieve better accuracy on thick domains, we propose to use polynomial test functions instead of Fourier series. We also propose to improve the solution by various regularization techniques that are tested and compared. Numerical assessments are provided in 2D and 3D.

Keywords: crack identification; reciprocity gap method; inverse problem; Fourier series; harmonic polynomials.

1 Introduction

The detection of cracks in working devices is an important issue in mechanical engineering. In the frame of this work, we focus on the identification of cracks in the linear elastostatic regime; we suppose that in-site measurements give us access to the displacement and traction fields on the boundary of the device. The bibliography related to crack identification mostly provides theoretical results on 2D domains: a uniqueness result for a buried crack can be found in [14], uniqueness and local Lipschitz stability results have been established for emerging cracks in [5] and [12]. Few uniqueness results exist in the 3D framework; they all require the knowledge of all the possible measurements [13]. Note that a numerical study was carried out in [1] for crack front identification from tangential surface displacements measurements. In [16], a crack identification problem was addressed by the resolution of two Cauchy problems.

Regarding the practical computation of the crack, the well-known reciprocity gap method, introduced in [2], provides explicit semi-analytical formulas able to deduce the form of a crack from over specified measurements. Theoretical results were given in [4] in the 3D elasticity framework. In [22], the authors studied the case of linear anisotropic 3D elasticity with a variant of the original method. In [20], another variant was proposed to find ellipsoidal inclusions in a 3D domain. In [21] an application of the reciprocity principle for the determination of planar cracks in piezoelectric material was given and 2D numerical test cases were carried out.

However, as far as the authors know, there has never been any paper in the literature that handles this issue numerically on a 3D elastostatic domain with unknown crack plane. Numerical results for 2D identification problems with the Laplace equation are given in [6, 9]. In [1], a 3D case with incomplete measurements is considered, but the crack is emerging and its plane is given. In [7] an alternative way to reconstruct the crack without the Fourier functions was proposed. In [8], results are provided for the Helmholtz equation on a 3D geometry; thanks to the conditional well-posedness of the inverse problem on this equation, it is possible to choose only the largest wave lengths, which prevents high oscillations of the displacement jump over the crack.

In this contribution, we propose to study the reciprocity gap algorithm given in [4] in order to determine and to overcome its limits. In Section 2, the reciprocity gap method for 3D elastostatic problems is recalled and the main flaw of the proposed Fourier reconstruction is highlighted. In Section 3, a polynomial reconstruction is proposed to overcome the sensibility to noise of the Fourier approach. Section 4 presents various regularization strategies. Section 5 contains numerical assessments of the variants on both 2D and 3D problems.

2 The reciprocity gap method and its classical implementation

In this section, we recall the reciprocity gap method proposed in [3, 4] for the detection of planar cracks. We show that one of its ingredients, namely the Fourier approximation of the displacement jump, may lead to practical difficulties in the case of thick domains.

2.1 General principle of the reciprocity gap method

Let $\Omega \subset \mathbb{R}^d$ be a regular open domain ($d = 2$ or 3). Our objective is to identify a non-emerging planar crack characterized by its surface $\Sigma \subset \omega = \Omega \cap \Pi$ where Π is a plane, $\Sigma \cap \partial\Omega = \emptyset$, from the knowledge of all the boundary conditions on $\partial\Omega$. See Figure 1 for a representation of the geometrical entities.

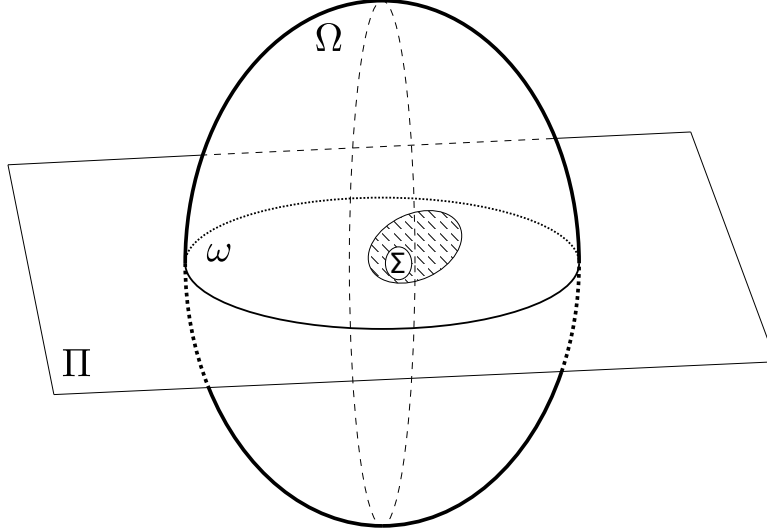


Figure 1: Buried planar crack

Following [4], we consider a static linear elasticity problem in small strain. Let \underline{u} be the displacement field, $\underline{\varepsilon}$ the symmetric gradient operator, $\underline{\sigma}$ the Cauchy stress tensor, \mathbb{H} the tensor of Hooke, \underline{n} the outer-pointing normal vector, \underline{n}_Π a unit vector orthogonal to Π .

A displacement field \underline{u} which solves the mechanical system:

$$\begin{aligned} \operatorname{div}(\underline{\sigma}) &= \underline{0} \quad \text{in } \Omega \setminus \Sigma \\ \underline{\sigma} &= \mathbb{H} : \underline{\varepsilon}(\underline{u}) \\ \underline{\sigma} \cdot \underline{n}_\Pi &= \underline{0} \quad \text{on } \Sigma \end{aligned} \quad (1)$$

can be characterized by the following traces:

$$\begin{aligned} \hat{\underline{u}} &:= \underline{u}|_{\partial\Omega} \\ \hat{\underline{f}} &:= \underline{\sigma} \cdot \underline{n} \quad \text{on } \partial\Omega \end{aligned} \quad (2)$$

Note that the Neumann condition $\hat{\underline{f}}$ satisfies the compatibility conditions:

$$\int_{\partial\Omega} \hat{\underline{f}} \, dS = \underline{0} \quad \text{and} \quad \int_{\partial\Omega} \underline{x} \times \hat{\underline{f}} \, dS = \underline{0} \quad (3)$$

The aim of the Reciprocity Gap method is to infer Σ from the knowledge of a family of boundary values $(\hat{\underline{u}}_r, \hat{\underline{f}}_r)_r$; in practice two experiments are enough so that $r \in \{1, 2\}$.

For a couple $(\hat{\underline{u}}_r, \hat{\underline{f}}_r)$, we define the reciprocity gap functional RG_r :

$$\begin{aligned} \operatorname{RG}_r &: H^1(\Omega) \rightarrow \mathbb{R} \\ \underline{v} &\mapsto \operatorname{RG}_r(\underline{v}) = \int_{\partial\Omega} (\hat{\underline{f}}_r \cdot \underline{v} - \hat{\underline{u}}_r \cdot \underline{\sigma}(\underline{v}) \cdot \underline{n}) \, dS \end{aligned} \quad (4)$$

where we use the notation $\underline{\underline{\sigma}}(\underline{v}) = \mathbb{H} : \underline{\underline{\varepsilon}}(\underline{v})$.

Let $\mathcal{V} = \{\underline{v} \in H^1(\Omega), \operatorname{div}(\underline{\underline{\sigma}}(\underline{v})) = \underline{0} \text{ weakly in } \Omega\}$. \mathcal{V} is the mechanical counterpart to the set of “harmonic” functions in the uncracked domain. We have the following property:

$$\forall \underline{v} \in \mathcal{V}, \quad \operatorname{RG}_r(\underline{v}) = \int_{\Sigma} \underline{\underline{\sigma}}(\underline{v}) : (\underline{n}_{\Pi} \otimes \llbracket \underline{u}_r \rrbracket) \, \mathrm{dS} \quad (5)$$

where $\llbracket \underline{u}_r \rrbracket$ is the jump of displacement on the crack, which is different from zero in the case of an opening crack. The study of the functionals (RG_r) (if necessary for different r) can thus provide information on \underline{n}_{Π} , Π and finally Σ which is the support of $\llbracket \underline{u}_r \rrbracket$ in Π . Note that Σ does not need to be connected.

2.2 Determination of the normal to the crack plane

Let (\underline{e}_i) be the canonical basis of \mathbb{R}^3 , and (x_i) the components of the vector \underline{x} . Let us define six test-fields $(\underline{v}_{ij})_{1 \leq i \leq j \leq 3}$:

$$\underline{v}_{ij} \text{ is such that } \underline{\underline{\sigma}}(\underline{v}_{ij}) = (\underline{e}_i \otimes \underline{e}_j^T)_{sym} \quad (6)$$

Depending on the space variations of \mathbb{H} , the expressions for (\underline{v}_{ij}) may be tedious to derive. Next remark gives them in the simplest case.

Remark 1 (Expression of (\underline{v}_{ij}) in the homogeneous isotropic case). Let E be the Young modulus and ν be the Poisson coefficient, we have:

$$\begin{aligned} \underline{v}_{11} &= \frac{1}{E} \begin{pmatrix} x_1 \\ -\nu x_2 \\ -\nu x_3 \end{pmatrix} & \underline{v}_{22} &= \frac{1}{E} \begin{pmatrix} -\nu x_1 \\ x_2 \\ -\nu x_3 \end{pmatrix} & \underline{v}_{33} &= \frac{1}{E} \begin{pmatrix} -\nu x_1 \\ -\nu x_2 \\ x_3 \end{pmatrix} \\ \underline{v}_{12} &= \frac{1+\nu}{2E} \begin{pmatrix} x_2 \\ x_1 \\ 0 \end{pmatrix} & \underline{v}_{13} &= \frac{1+\nu}{2E} \begin{pmatrix} x_3 \\ 0 \\ x_1 \end{pmatrix} & \underline{v}_{23} &= \frac{1+\nu}{2E} \begin{pmatrix} 0 \\ x_3 \\ x_2 \end{pmatrix} \end{aligned} \quad (7)$$

We then assemble the symmetric matrix $\tilde{\mathbf{R}}_r$ with $\tilde{\mathbf{R}}_{r,ij} = \operatorname{RG}_r(\underline{v}_{ij})$. We have:

$$\tilde{\mathbf{R}}_r = \left(\left(\int_{\Sigma} \llbracket \underline{u}_r \rrbracket \, \mathrm{dS} \right) \underline{n}_{\Pi}^T \, \mathrm{dS} \right)_{sym} \quad (8)$$

We note $\tilde{\underline{U}}_r = \int_{\Sigma} \llbracket \underline{u}_r \rrbracket \, \mathrm{dS}$. The objective is to determine \underline{n}_{Π} from the knowledge of $\tilde{\mathbf{R}}_r$. In order to tell \underline{n}_{Π} from $\tilde{\underline{U}}_r$ we need two experiments; in fact we determine $(\underline{n}_{\Pi}, \tilde{\underline{U}}_1, \tilde{\underline{U}}_2)$ from $(\tilde{\mathbf{R}}_1, \tilde{\mathbf{R}}_2)$.

We propose a slightly different technique for the computation of \underline{n}_{Π} than what was given in [4], it relies on one singular values decomposition instead of two and the same method applies in both 2D and 3D. We have the following properties:

$$\operatorname{tr}(\tilde{\mathbf{R}}_r) = \tilde{\underline{U}}_r \cdot \underline{n}_{\Pi} \quad \text{and} \quad \|\tilde{\mathbf{R}}_r\|_F^2 = \operatorname{tr}(\tilde{\mathbf{R}}_r^T \tilde{\mathbf{R}}_r) = \frac{1}{2} \left((\tilde{\underline{U}}_r \cdot \underline{n}_{\Pi})^2 + \|\tilde{\underline{U}}_r\|_2^2 \right) \quad (9)$$

We can then compute $\|\tilde{\underline{U}}_r\|_2$ and define the normalized quantities $\mathbf{R}_r = \tilde{\mathbf{R}}_r / \|\tilde{\underline{U}}_r\|_2$ which is associated to $\underline{U}_r = \tilde{\underline{U}}_r / \|\tilde{\underline{U}}_r\|_2$. We compute:

$$\begin{aligned} \gamma_r &:= \operatorname{tr}(\mathbf{R}_r) = \underline{U}_r \cdot \underline{n}_{\Pi} \\ \gamma_{12} &:= 2 \operatorname{tr}(\mathbf{R}_1 \mathbf{R}_2) - \gamma_1 \gamma_2 = \underline{U}_1 \cdot \underline{U}_2 \\ \mathbf{\Delta}_1 &:= (\mathbf{R}_1 \mathbf{R}_2 - \gamma_2 \mathbf{R}_1) - \frac{\gamma_{12} - \gamma_1 \gamma_2}{4} \mathbf{I} \end{aligned} \quad (10)$$

Then \underline{n}_{Π} spans the null space of $\mathbf{\Delta}_1$, it can be computed using a singular value decomposition.

Note that for the rest of the identification, one single set of measurement is enough. We keep the notation r but in practice, it only takes one value ($r = 1$ or $r = 2$).

2.3 Determination of the crack plane

Let $(\underline{t}_1, \underline{t}_2)$ be an orthonormal basis of \underline{n}_Π^\perp . In the frame $(\underline{t}_1, \underline{t}_2, \underline{n}_\Pi)$, the coordinates are written (X_1, X_2, X_3) , and the equation of Π is $X_3 = C$, with C a constant to be determined. The origin of the frame is chosen so that Ω is in the upper semi-space ($X_3 > 0$), this implies that $C > 0$.

We build test fields $(\underline{v}_1, \underline{v}_2)$ such that $\underline{\sigma}(\underline{v}_i) = X_3(\underline{t}_i \otimes \underline{n}_\Pi)_{sym}$ for $i \in \{1, 2\}$. They lead to:

$$\text{RG}_r(\underline{v}_i) = C \left(\int_\Sigma \llbracket \underline{u}_r \rrbracket \, dS \right) \cdot \underline{t}_i \quad (11)$$

and we have:

$$\text{RG}_r(\underline{v}_1)^2 + \text{RG}_r(\underline{v}_2)^2 = C^2 \left(\|\tilde{\underline{U}}_r\|_2^2 - (\tilde{\underline{U}}_r \cdot \underline{n}_\Pi)^2 \right) \quad (12)$$

which enables to compute C , using the values from (9).

Remark 2 (Expression of (\underline{v}_i) in the 3D isotropic homogeneous case).

$$\underline{v}_1 = \begin{pmatrix} -\frac{X_1^2}{2E} - \nu \frac{X_2^2}{2E} + (2 + \nu) \frac{X_3^2}{2E} \\ \nu \frac{X_1 X_2}{E} \\ \nu \frac{X_1 X_3}{E} \end{pmatrix} \quad \underline{v}_2 = \begin{pmatrix} \nu \frac{X_1 X_2}{E} \\ -\frac{X_2^2}{2E} - \nu \frac{X_1^2}{2E} + (2 + \nu) \frac{X_3^2}{2E} \\ \nu \frac{X_1 X_3}{E} \end{pmatrix} \quad (13)$$

Remark 3 (Expression of \underline{v}_1 in the 2D plane stress case).

$$C = \frac{|\text{RG}_r(\underline{v}_1)|}{\sqrt{\|\tilde{\underline{U}}_r\|_2^2 - (\tilde{\underline{U}}_r \cdot \underline{n}_\Pi)^2}} \quad \text{with} \quad \underline{v}_1 = \begin{pmatrix} -\frac{X_1^2}{2E} + (2 + \nu) \frac{X_3^2}{2E} \\ \nu \frac{X_1 X_3}{E} \end{pmatrix} \quad (14)$$

2.4 Determination of the crack itself

The crack Σ can be characterized as the support of $\llbracket \underline{u}_r \rrbracket$ in $\omega = \Pi \cap \Omega$. The idea is thus to identify $\llbracket \underline{u}_r \rrbracket$. In [4], the authors proposed test-fields that permit to approximate both the normal and of the tangential parts of $\llbracket \underline{u}_r \rrbracket$. In order to simplify the presentation, we assume that the test case r is opening the crack, so that identifying the normal part of the displacement jump is enough.

The method relies on the possibility to build N functions $(\underline{\phi}_j)$ in \mathcal{V} which generate pure opening stress in the plane ω :

$$\text{for } \underline{\phi}_j \in \mathcal{V}, \exists \varphi_j \in L^2(\omega) \quad \underline{\sigma}(\underline{\phi}_j)(X_1, X_2, 0) = \varphi_j(X_1, X_2) \underline{n}_\Pi \otimes \underline{n}_\Pi \quad (15)$$

Then a Petrov-Galerkin approach can be employed: the displacement jump is approximated as a linear combination: $\llbracket \underline{u}_r \rrbracket \cdot \underline{n}_\Pi \simeq \sum_{i=1}^N u_i \tilde{\varphi}_i$ (in general $\tilde{\varphi}_i = \varphi_i$), the unknown coefficients (u_i) being determined by the reciprocity gap equation ((4),(5)) tested against functions $(\underline{\phi}_j)$:

$$\forall j \in \llbracket 1, N \rrbracket, \sum_{i=1}^N u_i \int_\omega \tilde{\varphi}_i(X_1, X_2) \varphi_j(X_1, X_2) \, dS = \text{RG}_r(\underline{\phi}_j) \quad (16)$$

which is a classical $N \times N$ linear system which can be written under the form:

$$\mathbf{B}_N \mathbf{u}_N = \mathbf{b}_N \quad \text{with} \quad \begin{aligned} \mathbf{u}_N &: \text{vector of } (u_i), & \mathbf{b}_N &: \text{vector of } (\text{RG}_r(\underline{\phi}_j)) \\ \mathbf{B}_N &: \text{matrix of } \int_\omega \tilde{\varphi}_i(X_1, X_2) \varphi_j(X_1, X_2) \, dS & & 1 \leq i, j \leq N \end{aligned} \quad (17)$$

The preparation of this system only implies surface integrations on ω for the left-hand side and on $\partial\Omega$ for the right-hand side.

2.4.1 Approximation by Fourier expansion

In [4] it is proposed to develop the displacement jump in Fourier series. First a translation $X_3 \leftarrow X_3 - C$ is operated so that Π corresponds to $X_3 = 0$. In the case of homogeneous behavior, it is possible to derive a family of functions $(\underline{\phi}_{k,l})$ (see the remark 4 for the actual expression in the isotropic case) such that we have:

$$\underline{\sigma}(\underline{\phi}_{k,l}) \cdot \underline{n}_\Pi = e^{-2i\pi\left(\frac{kX_1}{L_1} + \frac{lX_2}{L_2}\right)} \underline{n}_\Pi \text{ in } \Pi$$

where L_1 and L_2 are the lengths of a rectangle enclosing ω , that should be taken as small as possible. The displacement jump is decomposed in Fourier series:

$$\llbracket \underline{u}_r \rrbracket \cdot \underline{n}_\Pi = \sum_{k,l} u_{k,l} \tilde{\varphi}_{k,l} \quad \text{with} \quad \tilde{\varphi}_{k,l} = e^{2i\pi\left(\frac{kX_1}{L_1} + \frac{lX_2}{L_2}\right)}$$

Thanks to classical orthogonality properties between the Fourier functions in a rectangular domain, the linear system to be solved is diagonal, and the Fourier coefficients $(u_{k,l})$ are straightforward to compute:

$$u_{k,l} = \frac{\text{RG}_r(\underline{\phi}_{k,l})}{L_1 L_2} \quad (18)$$

Remark 4 (Expression of $\underline{\phi}_{k,l}$ in the 3D homogeneous isotropic case).

$$\underline{\phi}_{k,l} = \frac{1 + \nu}{2E\lambda_3^2} \begin{pmatrix} -i\lambda_1 e^{-i\lambda_1 X_1 - i\lambda_2 X_2} (e^{\lambda_3 X_3} + e^{-\lambda_3 X_3}) \\ -i\lambda_2 e^{-i\lambda_1 X_1 - i\lambda_2 X_2} (e^{\lambda_3 X_3} + e^{-\lambda_3 X_3}) \\ \lambda_3 e^{-i\lambda_1 X_1 - i\lambda_2 X_2} (e^{\lambda_3 X_3} - e^{-\lambda_3 X_3}) \end{pmatrix} \quad \text{with} \quad \begin{matrix} \lambda_1 = \frac{2k\pi}{L_1} \\ \lambda_2 = \frac{2l\pi}{L_2} \end{matrix} \quad \text{and} \quad \lambda_3 = \sqrt{\lambda_1^2 + \lambda_2^2} \quad (19)$$

2.4.2 Discussion

Fourier series are extremely interesting because they result in a diagonal system. Anyhow they trigger certain difficulties:

- As $\text{RG}(\underline{\phi}_{k,l})$ involves surface integrals of cosine functions, a high number of Gauss point must be employed in order to approximate them properly, in particular if high orders (large (k, l)) are employed.
- The function $\underline{\phi}_{k,l}$ have a (real) exponential dependence in the normal direction (X_3). This gives more importance to measurements far from the crack Σ and this may strongly amplify the noise in the data. This problem is thus particularly important for thick domains.

So, the mildness of the linear system is counterbalanced by the fact that the evaluation of the right-hand side increases rapidly in difficulty with the order of the Fourier development. A straightforward regularization technique for this method is then to limit the number of modes in the Fourier decomposition of the reconstructed $\llbracket \underline{u}_r \rrbracket$. As for any regularizing technique, the number of Fourier modes should be chosen to realize a compromise between the precision and the amplification of the noise.

3 Proposition of a new polynomial approximation method

As seen in previous section, it would be profitable to use a new approximation basis which would limit the amplification of the noise. In this section we investigate the use of polynomials. Such functions have the advantage to be easy to integrate exactly (with a sufficient amount of Gauss points), and to grow slower than exponentials.

As before, we assume that the reconstruction of $\llbracket \underline{u}_r \rrbracket \cdot \underline{n}_\Pi$ is enough to recover Σ . Studying the tangential part of the displacement jump seems not to pose any extra difficulty with the polynomial approach that we develop.

As usual, the first task is to normalize the coordinates in the crack plane: we build a bounding box of Ω whose sides are aligned with $(t_1, t_2, \underline{n}_\Pi)$. Let (L_1, L_2, L_3) be the half-length of the sides. We write $(\tilde{x}_1, \tilde{x}_2, \tilde{x}_3)$ the scaled coordinates so that a point of Ω belongs to the unit cube.

We use multiindex notations for polynomials:

$$\boldsymbol{\alpha} = (\alpha_1, \alpha_2, \alpha_3) \in \mathbb{N}^3, \quad \tilde{\mathbf{x}}^\alpha = \tilde{x}_1^{\alpha_1} \tilde{x}_2^{\alpha_2} \tilde{x}_3^{\alpha_3}, \quad |\boldsymbol{\alpha}| = \sum_i \alpha_i$$

3.1 Construction of “harmonic” polynomials

Let \mathcal{P}_n be the space of polynomials of degree inferior or equal to n with values in \mathbb{R}^d . The polynomial $\underline{A} \in \mathcal{P}_n$ takes the form $\underline{A}(\tilde{\mathbf{x}}) = \sum_{\boldsymbol{\alpha} \leq n} \underline{a}_\alpha \tilde{\mathbf{x}}^\alpha$ where \underline{a}_α are the coefficients which characterize \underline{A} . \mathcal{P}_n is a space of dimension $d \binom{n+d}{n}$. In our experiments n will typically be 20, leading to a space of dimension 5313. In order to manipulate the polynomial, we write the coefficients \underline{a}_α in column-vector form \mathbf{a}_α .

In order to work inside $\mathcal{V} \cap \mathcal{P}_n$, we need to satisfy the condition $\text{div}(\sigma(\underline{A})) = 0$ which leads to (dn) homogeneous linear equations on the coefficients (\underline{a}_α) . We use a symbolic calculus software in order to compute the matrix $\boldsymbol{\Delta}_n$ associated with the stress-divergence operator in \mathcal{P}_n , the divergence-free conditions translate into a condition on the coefficients:

$$\boldsymbol{\Delta}_n \mathbf{a}_\alpha = \mathbf{0} \quad (20)$$

Thus we characterize the polynomials in $\mathcal{V} \cap \mathcal{P}_n$ as the ones whose coefficients span the kernel of $\boldsymbol{\Delta}_n$. All these polynomials can be used as test functions in the reciprocity gap equation (16), anyhow, we prefer to restrict to polynomials also suited for the approximation of the displacement jump.

Among the polynomials, we are more interested in the ones which are non-zero on Π . For each pair of non-negative integers (α_1, α_2) with $\alpha_1 + \alpha_2 \leq n$, we propose to build one function $(\underline{\phi}_{\alpha_1, \alpha_2})$, such that:

$$\underline{\phi}_{\alpha_1, \alpha_2} \in \mathcal{V} \cap \mathcal{P}_n, \quad \underline{\sigma}(\underline{\phi}_{\alpha_1, \alpha_2}) = \tilde{x}_1^{\alpha_1} \tilde{x}_2^{\alpha_2} \underline{n}_\Pi \otimes \underline{n}_\Pi \text{ on } \Pi \quad (21)$$

Let $\mathbf{a}_{\alpha_1, \alpha_2}$ be the vector of coefficients of $\underline{\phi}_{\alpha_1, \alpha_2}$, and let $\boldsymbol{\chi}_{\alpha_1, \alpha_2}$ be the operator which computes the coefficient associated with the monomial $\tilde{x}_1^{\alpha_1} \tilde{x}_2^{\alpha_2}$ of the stress in Π . The coefficients $\mathbf{a}_{\alpha_1, \alpha_2}$ must be solution to the following equation:

$$\begin{pmatrix} \boldsymbol{\Delta}_n \\ \boldsymbol{\chi}_{\alpha_1, \alpha_2} \end{pmatrix} \mathbf{a}_{\alpha_1, \alpha_2} = \begin{pmatrix} \mathbf{0} \\ 1 \end{pmatrix} \quad (22)$$

Note that these conditions are not enough to fully characterize $\underline{\phi}_{\alpha_1, \alpha_2}$ since the function is defined up to polynomials with zero normal stress on Π (whose coefficients span the kernel of the matrix of (22)):

$$\mathcal{N} = \left\{ \underline{\psi} \in \mathcal{V} \cap \mathcal{P}_n, \underline{\sigma}(\underline{\psi}) \cdot \underline{n}_\Pi = 0 \text{ on } \Pi \right\} \neq \emptyset \quad (23)$$

Various strategy can be imagined to choose the components in \mathcal{N} , one possibility is presented in the next subsection.

The displacement jump is approximated under the form $\llbracket \underline{u}_r \rrbracket \cdot \underline{n}_\Pi(\tilde{x}_1, \tilde{x}_2) \simeq \sum u_{\alpha_1, \alpha_2} \tilde{x}_1^{\alpha_1} \tilde{x}_2^{\alpha_2}$, the (u_{α_1, α_2}) are solutions to a system of the form (17):

$$\forall (\beta_1, \beta_2) > 0, (\beta_1 + \beta_2) \leq n, \quad \sum_{\alpha_1 + \alpha_2 \leq n} u_{\alpha_1, \alpha_2} \int_\omega \tilde{x}_1^{\alpha_1} \tilde{x}_2^{\alpha_2} \tilde{x}_1^{\beta_1} \tilde{x}_2^{\beta_2} dS = \text{RG}_r(\underline{\phi}_{\beta_1, \beta_2}) \quad (24)$$

3.2 Simplified construction in the 3D case

As pointed out, \mathcal{P}_n is a huge space. It appeared that a good subspace could be intuited. Instead of dealing with general polynomials in the canonical basis, we propose to start from polynomials of the form:

$$\underline{\phi}_{k,l} = \begin{pmatrix} \sum_{i=0}^{\lfloor (k+1)/2 \rfloor} \sum_{j=0}^{\lfloor l/2 \rfloor} a_{i,j}^1 \tilde{x}_1^{k+1-2i} \tilde{x}_2^{l-2j} \tilde{x}_3^{2i+2j} \\ \sum_{i=0}^{\lfloor k/2 \rfloor} \sum_{j=0}^{\lfloor (l+1)/2 \rfloor} a_{i,j}^2 \tilde{x}_1^{k-2i} \tilde{x}_2^{l+1-2j} \tilde{x}_3^{2i+2j} \\ \sum_{i=0}^{\lfloor k/2 \rfloor} \sum_{j=0}^{\lfloor l/2 \rfloor} a_{i,j}^3 \tilde{x}_1^{k-2i} \tilde{x}_2^{l-2j} \tilde{x}_3^{2i+2j+1} \end{pmatrix} \quad (25)$$

where $\lfloor \bullet \rfloor$ represents the floor function.

For a given pair (k, l) , we choose to build only one function $\underline{\phi}_{k,l}$. This means that we need to fully characterize the coefficients $(a_{i,j}^m)$ in (25).

Let $\mathbf{a}_{k,l}$ be the vector of the coefficients $(a_{i,j}^m)$ characterizing the function $\underline{\phi}_{k,l}$, the coefficients must satisfy the constraint (22), in a form adapted to the considered basis (25):

$$\begin{pmatrix} \Delta_{k,l} \\ \chi_{k,l} \end{pmatrix} \mathbf{a}_{k,l} = \begin{pmatrix} \mathbf{0} \\ 1 \end{pmatrix} \quad (26)$$

Since this constraint is not enough in order to fully characterize $\underline{\phi}_{k,l}$, we add a simple optimality condition:

$$\text{Minimize } \mathbf{a}_{k,l}^T \mathbf{M} \mathbf{a}_{k,l} \text{ under constraint (26)} \quad (27)$$

We tried several ideas for matrix \mathbf{M} . In the end we adopted the identity matrix. This means that we assume that the best polynomials have coefficients with similar magnitude. None of the other matrices we tried (penalizing the mechanical energy of the field, or the higher order terms in \tilde{x}_3) gave better results.

In practice, since the constraint matrix is not so large, it appeared to be more stable to search for $\mathbf{a}_{k,l}$ under the form $\mathbf{a}_{k,l} = \mathbf{a}_{k,l}^0 + \mathbf{C}_{k,l} \tilde{\mathbf{a}}_{k,l}$ where $\mathbf{a}_{k,l}^0$ satisfies the constraint and $\mathbf{C}_{k,l}$ is a basis of the right null space of the constraint matrix (26); $\tilde{\mathbf{a}}_{k,l}$ is then obtained by an unconstrained minimization. Note that $\mathbf{C}_{k,l}$ can be computed at a limited cost by recombining the null space of Δ_n which can be computed once for all.

Once the functions $(\underline{\phi}_{k,l})$ are determined, a small system of the same form as (17) can be obtained and solved.

3.3 Simplified construction for 2D plane stress

We propose the following test fields (x_1 is the tangent direction, x_3 is the normal, in order to limit the complexity of the equations, it is assumed that $L_1 = L_3$):

$$\underline{\phi}_k = \begin{pmatrix} \sum_{i=0}^{\lfloor k+1/2 \rfloor} a_i^1 \tilde{x}_1^{k+1-2i} \tilde{x}_3^{2i} \\ \sum_{i=0}^{\lfloor k/2 \rfloor} a_i^3 \tilde{x}_1^{k-2i} \tilde{x}_3^{2i+1} \end{pmatrix} \quad (28)$$

The conditions lead to:

- $\underline{\underline{\sigma}}(\underline{\phi}_k) = \tilde{x}_1^k \tilde{x}_3^l$ on $\tilde{x}_3 = 0 \quad \Rightarrow \quad a_0^1 = -\frac{1 - \nu^2}{\nu E(k+1)}$
- $\text{div}(\underline{\underline{\sigma}}(\underline{\phi}_k)) \cdot \mathbf{e}_1 = 0 \quad \Rightarrow \quad \forall 0 \leq i \leq \left\lfloor \frac{k-1}{2} \right\rfloor,$

$$\frac{a_i^1(k+1-2i)(k-2i) + a_i^3(2i+1)(k-2i)}{1-\nu^2} + \frac{a_{i+1}^1(2i+2)(2i+1) + a_i^3(k-2i)(2i+1)}{2(1+\nu)} = 0$$
- $\text{div}(\underline{\underline{\sigma}}(\underline{\phi}_k)) \cdot \mathbf{e}_3 = 0 \quad \Rightarrow \quad \forall 1 \leq i \leq \left\lfloor \frac{k}{2} \right\rfloor,$

$$\frac{a_i^3(2i)(k+1-2i) + a_i^1(2i)(k-2i+1)}{1-\nu^2} + \frac{a_{i-1}^3(k-2i+2)(k-2i+1) + a_i^1(k+1-2i)(2i)}{2(1+\nu)} = 0$$

(29)

There is just one less equation than unknowns. For that reason, and given the very satisfactory results obtained in section 5 for the 2D test-cases, it was simply decided to add the condition $a_0^3 = 0$ to close the system.

Once the functions $(\underline{\phi}_k)$ determined, a small system of the same form as (17) can be obtained and solved.

4 Regularization strategies for the identification of the crack

Previous section presented how to build polynomial subspaces of the search space \mathcal{V} (starting either from the full \mathcal{P}_n basis or from a simplified subspace basis). In any case, this resulted in linear system (17) to be solved which is not diagonal, contrary to the classical Fourier approximation (18). Even if the condition number is expected to grow with the dimension of the search space, we expect the quality of the right-hand side to be much improved by the use of polynomials.

Let us reuse the generic notations of 2.4 with single index. We assume that we have built N displacement functions $(\underline{\phi}_j)$ in \mathcal{V} . We assume the functions are sorted with increasing degree. Each function $\underline{\phi}_j$ generates pure normal stress on ω with intensity φ_j . The displacement jump is approximated as $\sum_{i=1}^N u_i \tilde{\varphi}_i$ (for the polynomial method $\tilde{\varphi}_i = \varphi_i$, for the Fourier method $\tilde{\varphi}_i = \bar{\varphi}_i$) and the (u_i) are determined by the reciprocity gap equation (17) which we recall:

$$\mathbf{B}_N \mathbf{u}_N = \mathbf{b}_N \quad \text{with} \quad \begin{array}{l} \mathbf{u}_N : \text{vector of } (u_i), \quad \mathbf{b}_N : \text{vector of } (\text{RG}_r(\underline{\phi}_j)) \\ \mathbf{B}_N : \text{matrix of } \int_{\omega} \tilde{\varphi}_i(X_1, X_2) \varphi_j(X_1, X_2) \text{dS} \end{array} \quad 1 \leq i, j \leq N$$

We thus define the approximated displacement jump:

$$\delta_N = \sum_{i=1}^N u_i \tilde{\varphi}_i \simeq \llbracket u_r \rrbracket \cdot n_{\Pi} \quad (30)$$

It appears that the terms associated with the higher degrees are tainted by the noise and lead to poor information. Regularization should still be considered, and we detail different strategies.

4.1 Truncation of the basis

A first regularization technique consists in truncating the basis of approximation and only use the first K functions $(\underline{\phi}_j)$ and $(\tilde{\varphi}_i)$ (with $K < N$), this results in a restricted system $\mathbf{B}_K \mathbf{u}_K = \mathbf{b}_K$ (with obvious notations) and another approximation of the displacement jump $\delta_K = \sum_{i=1}^K u_i \tilde{\varphi}_i$.

Of course the question is how to choose K . This parameter has to be as high as possible in order to achieve the highest precision in the reconstruction of the field, but it has also to be sufficiently small in order not to lead to dramatic amplification of the unavoidable measurement noise and round-off errors in the computation. Many strategies are available to make this choice, and one could for example cite the L-curve method developed in [15] or the Morozov principle, proposed in [19]. In the scope of this study, it was chosen not to try to experiment those strategies and to determine rather the optimal parameter manually by seeking for the better looking solution.

4.2 A posteriori gradient optimization

The truncation is applied because the higher terms $(u_i)_{K+1 \leq i \leq N}$ can not be properly estimated by the reciprocity gap equation. Anyhow other criteria can be applied in order to enrich the approximation δ_K :

$$\delta_K^+ = \delta_K + \sum_{i=K+1}^N \hat{u}_i \hat{\varphi}_i \quad (31)$$

where the functions $(\hat{\varphi}_i)_{K+1 \leq i \leq N}$ are modified versions of the $(\tilde{\varphi}_i)_{K+1 \leq i \leq N}$ orthogonalized with respect to the $(\varphi_i)_{1 \leq i \leq K}$:

$$\forall k \in \llbracket K+1, N \rrbracket, \begin{cases} \hat{\varphi}_k = \tilde{\varphi}_k - \sum_{i=1}^K d_{k,i} \tilde{\varphi}_i \\ \text{with } \forall j \in \llbracket 1, K \rrbracket, \int_{\omega} \varphi_j \tilde{\varphi}_k \, dS = \sum_{i=1}^K d_{k,i} \int_{\omega} \varphi_j \tilde{\varphi}_i \, dS \end{cases} \quad (32)$$

so that the reciprocity gap can not be perturbed by the enrichment of the approximation.

The enrichment coefficients $(\hat{u}_i)_{K+1 \leq i \leq N}$ are then free to be chosen in order to optimize the solution. The displacement jump should be non-zero only in Σ , but the identification procedure is likely to produce oscillations in $\omega \setminus \Sigma$, it then makes sense to add a criterion aiming at limiting these oscillations, which can be measured by the gradient of the jump. We tried both L^2 and L^1 measurements for the gradient:

$$(\hat{u}_i)_{K+1 \leq i \leq N} = \arg \min_{(\hat{v}_i)} \|\nabla \delta_K + \sum_{i=K+1}^N \hat{v}_i \nabla \hat{\varphi}_i\|_{L^2(\omega)} \quad (33)$$

$$(\hat{u}_i)_{K+1 \leq i \leq N} = \arg \min_{(\hat{v}_i)} \|\nabla \delta_K + \sum_{i=K+1}^N \hat{v}_i \nabla \hat{\varphi}_i\|_{L^1(\omega)} \quad (34)$$

The L^2 norm has the advantage to lead to a classical linear system to be solved. The L^1 norm criterion can be tackled by a linear programming technique as available is software libraries. More details regarding the implementation of this minimization are available in appendix A.

4.3 Tikhonov regularization

This method does not rely on prior truncation. It rephrases the problem (17) as a minimization problem and it adds a regularizing term still aiming at limiting the oscillations. Again L^2 and L^1 measures are considered:

$$\mathbf{u}_{N,2} = \arg \min_{\mathbf{v}} \frac{1}{2} \mathbf{v}^T \mathbf{B}_N \mathbf{v} - \mathbf{v}^T \mathbf{b}_N + \mu \|\mathbf{D}_N \mathbf{v}\|_{L^2(\omega)}^2 \quad (35)$$

$$\mathbf{u}_{N,1} = \arg \min_{\mathbf{v}} \frac{1}{2} \mathbf{v}^T \mathbf{B}_N \mathbf{v} - \mathbf{v}^T \mathbf{b}_N + \mu \|\mathbf{D}_N \mathbf{v}\|_{L^1(\omega)} \quad (36)$$

where \mathbf{D}_N is the gradient operator: $\mathbf{D}_N \mathbf{u}_N = \sum_{i=1}^N u_i \nabla \tilde{\varphi}_i$ and μ is a weight between the satisfaction of the reciprocity gap and the minimization of the gradient.

Again, the quadratic case leads to a simple linear system for the computation of $\mathbf{u}_{N,2}$.

The L^1 norm is more complex to tackle, in particular because it can not be differentiated. A first possibility, described in [11] in the context of image restoration, is to use a regularized norm $L^{1,\epsilon}$ which we describe for a scalar function f :

$$\|f\|_{L^{1,\epsilon}(\omega)} = \int_{\omega} \sqrt{f^2 + \epsilon} \, dS \quad (37)$$

where $\epsilon > 0$ should remain sufficiently small. Using this perturbed norm, a Newton-Raphson algorithm can be applied to approximate the minimum (if needed with line-search).

A second minimization method for the L^1 case, also coming from the image restoration community, is based on the dualization of the problem and is presented on the annex B.

Note that convergence is ensured for neither algorithm. A possible, apparently reliable, criterion can be obtained by computing the distance between the solutions given by both algorithms.

5 Numerical assessments

The aim of this section is to evaluate the reciprocity gap method for the identification of buried cracks for 2D and 3D problems. In particular, the new polynomial basis is compared to the classical Fourier approximation, and the various regularization methods are tested.

In the following numerical experiments, the data are obtained from a direct finite element resolution (with second order triangle/tetrahedral Lagrange elements). The fields on the boundary are then extracted and potentially receive a Gaussian noise to simulate the measurement process. The integrals are computed on a boundary mesh with a high-order Gauss integration method so that all polynomials up to degree 20 are exactly integrated.

5.1 Identification of a line crack in a rectangular 2D domain

In this part, the method is numerically investigated for a 2D plane stress crack identification problem. We consider a cracked rectangular domain whose dimensions are $10 \text{ mm} \times h$ with $h \in [1, 15] \text{ mm}$. Two load cases are applied: they consist in (pure Neumann) tractions (\underline{f}_r) aligned with the axis. Dirichlet values (\underline{u}_r) are then extracted on $\partial\Omega$. The isotropic material has the following properties: Young modulus $E = 210,000 \text{ MPa}$ and Poisson ratio $\nu = 0.3$. Figure 2 shows the finite element mesh; it is refined on the boundary in order to have more precise interpolation of \underline{u}_r . While the side of an element in the center of the domain is around 0.5 mm , this size is 0.1 mm on the boundary. This results in 500 elements on the boundary and 10,537 nodes for the direct resolution. The same boundary mesh is used to compute the integrals. To compensate the fact that the direct and inverse resolution share the same boundary mesh, some cases were studied with the addition of synthetic noise on the boundary measurements. The reference 2D solutions of the direct problem for the two load cases are presented on figure 2.

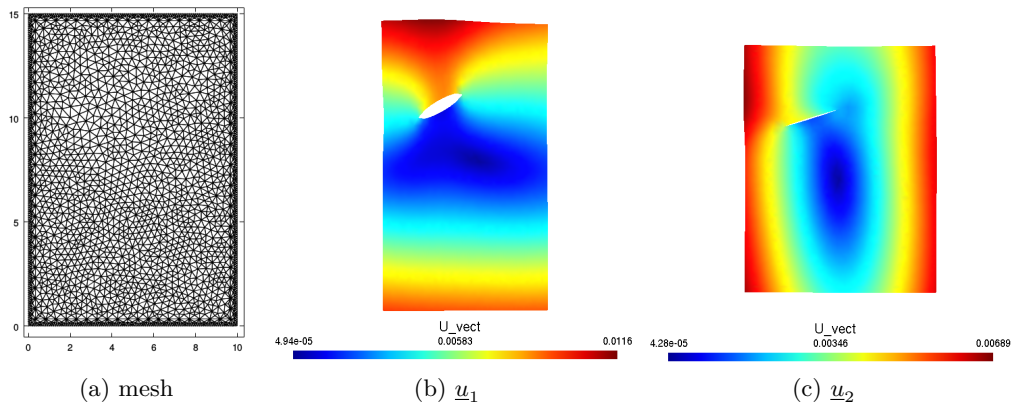


Figure 2: Example of FE mesh for the direct resolution, and solution (amplification $\times 100$)

As will be presented, the identification procedure in the 2D domain gives rather satisfying results. This is why the benefit of the regularization strategies is mainly discussed in the 3D case.

5.1.1 Identification of the normal and of the line

Figure 3 and 4 present the identification of the normal vector \underline{n}_Π and of the line Π in the noiseless case for a slim and a thick domain. For the identification of the line, the results obtained with the two load cases are both printed. The identification goes without major problem.

Figures 5 and 6 present the same experiments in the presence of 1% noise. In these cases, the normal is still well identified whereas the determination of the line is slightly more sensitive, in particular in the thin case and vertical load case. This can be explained by the formula (14), since in that case, the denominator tends to be small and amplifies errors.

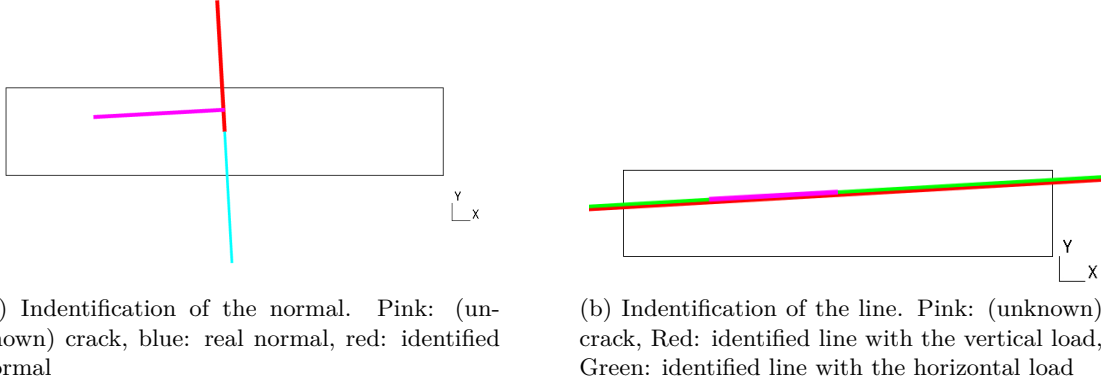


Figure 3: Thin 2D domain ($h = 2$ mm) in the absence of noise, identification of the line.

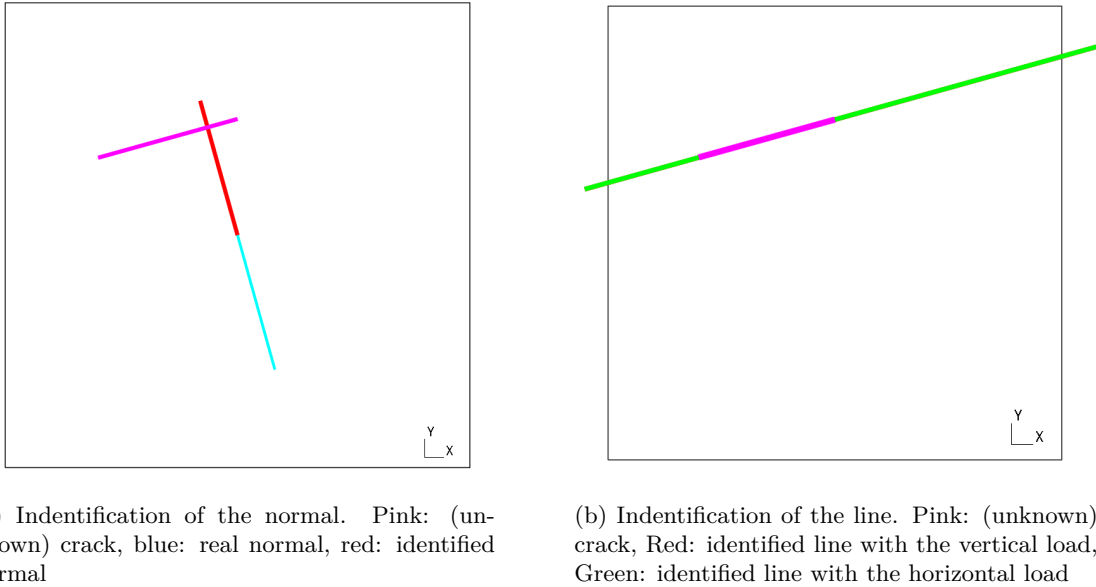


Figure 4: Thick 2D domain ($h = 10$ mm) in the absence of noise, identification of the line.

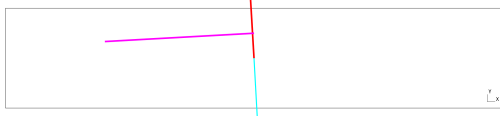
5.1.2 Identification of the crack

Figure 7 depicts the normal displacement jump $[[u_r]] \cdot n_\Pi$ on the crack line ($\omega = \Pi \cap \Omega$) using Fourier and polynomial approximations. As expected, for noiseless data, the reconstruction using polynomial functions is more accurate than the Fourier one. Only the polynomial technique is able to give results for very thick domains ($h \geq 10$ mm).

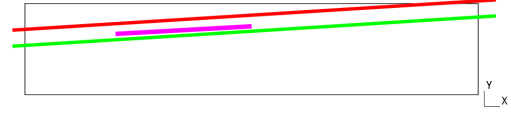
On Figure 8, we notice however that the numerical solutions obtained using polynomial functions are less stable with respect to the percentage of noise injected into the input displacement data \underline{u}_r , but this advantage of the Fourier functions disappears when the thickness of the domain increases.

On Table 1, the summary about the optimal polynomial degree or Fourier order and the obtained L^2 error for different thicknesses and noise levels can be found. The error is the relative error on the normal displacement jump, measured with $L^2(\omega)$ norm and is written $e_2(u)$. In practice, in this study, the optimal polynomial degree is tuned by hand by searching the value that gives the better looking solution.

Next we evaluate the effect of the richness of the available information on the quality of the reconstruction. On our synthetic experiment, the available information is a function of the density of the mesh used at the boundary for the generation of the direct solution, so the identification procedure is run on different meshes, presented on Figure 9. Each mesh size leads to the need of a different degree

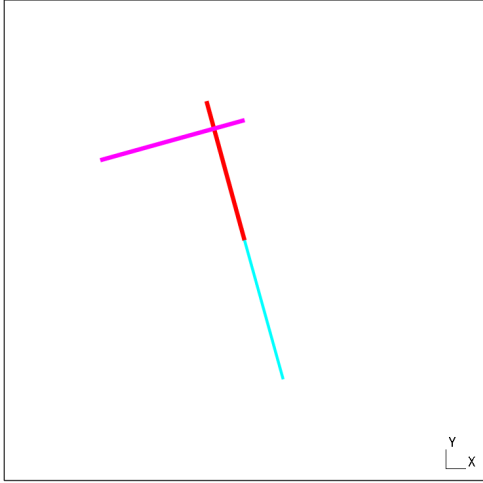


(a) Identification of the normal. Pink: (unknown) crack, blue: real normal, red: identified normal

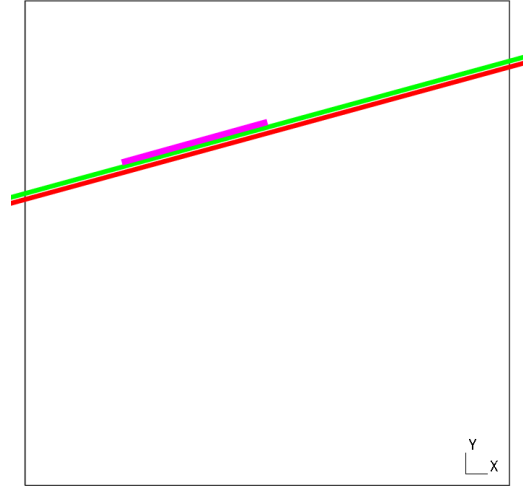


(b) Identification of the line. Pink: (unknown) crack, Red: identified line with the vertical load, Green: identified line with the horizontal load

Figure 5: Thin 2D domain ($h = 2$ mm) with 1% noise, identification of the line.



(a) Identification of the normal. Pink: (unknown) crack, blue: real normal, red: identified normal



(b) Identification of the line. Pink: (unknown) crack, Red: identified line with the vertical load, Green: identified line with the horizontal load

Figure 6: Thick 2D domain ($h = 10$ mm) with 1% noise, identification of the line.

of the polynomial leading to the optimal solution. Those informations can be found in Table 2.

The main conclusion we draw to is that when more information is available, the degree of the reconstruction polynomials can be increased and the precision of the identification improves.

thickness (mm)	noise level	optimal degree (polynomial)	L^2 error $e_2(u)$	optimal order (Fourier)	L^2 error $e_2(u)$
2	0	15	0.0072429	4	0.022424
2	0.01	10	0.023584	4	0.014851
2	0.1	3	0.60718	2	0.3828
3	0	14	0.016906	2	0.13844
4	0	10	0.017701	1	0.36841
5	0	10	0.026753	1	0.78623
10	0	8	0.049781	-	-
10	0.01	5	0.19486	-	-
15	0	5	0.15391	-	-

Table 1: Errors and optimal degree of polynomials or Fourier order for different test-cases

length of boundary elements $l_b(\text{mm})$	optimal polynomial degree	L^2 error $e_2(u)$
0.5	10	0.020010
0.4	10	0.016615
0.3	10	0.014982
0.2	15	0.011293
0.1	15	0.0072429

Table 2: Effect of the characteristic size of the mesh on the boundary for $h = 2$.

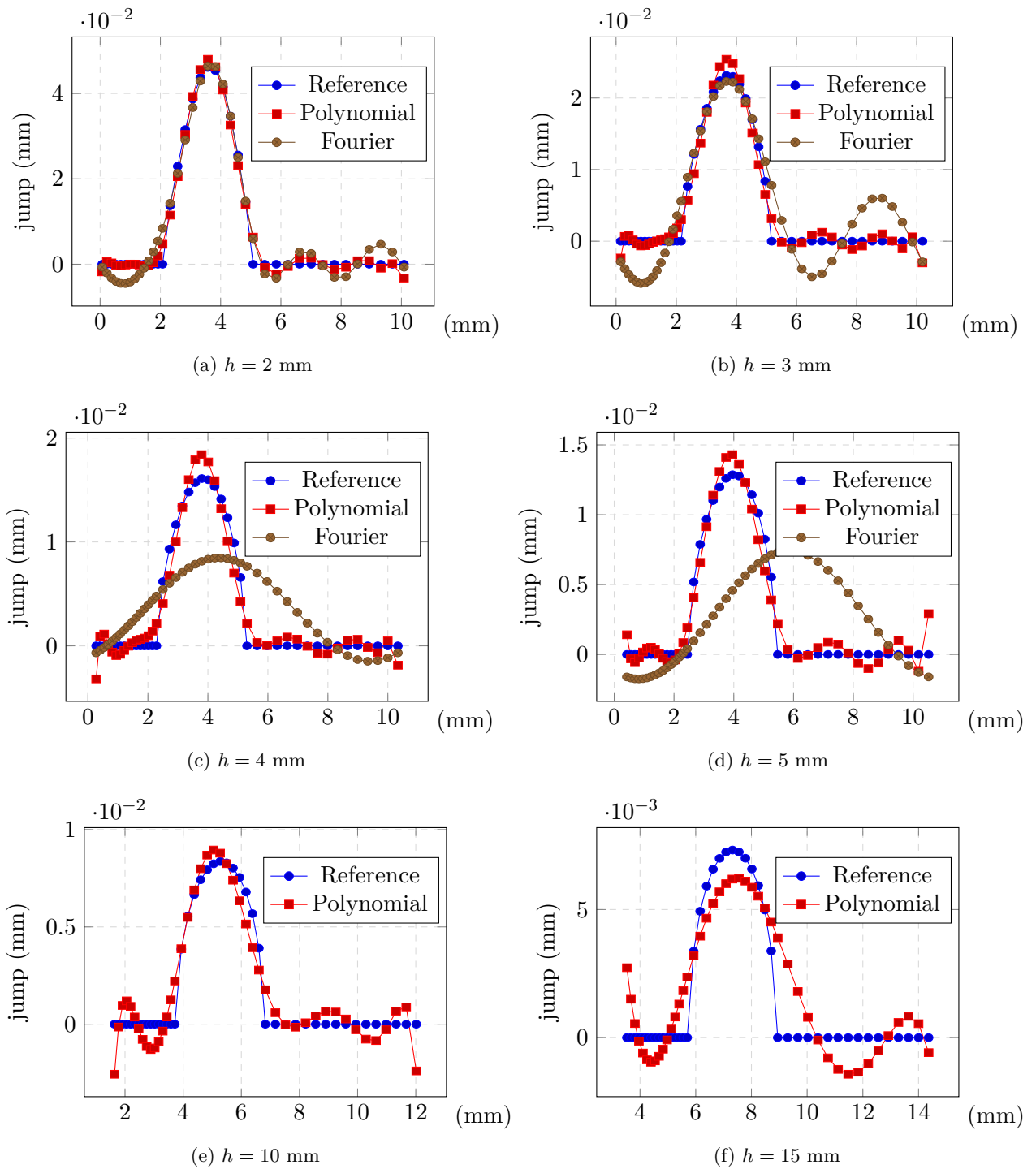


Figure 7: Identification of $[[u_r]] \cdot n_{II}$ in ω for various thicknesses in the absence of noise

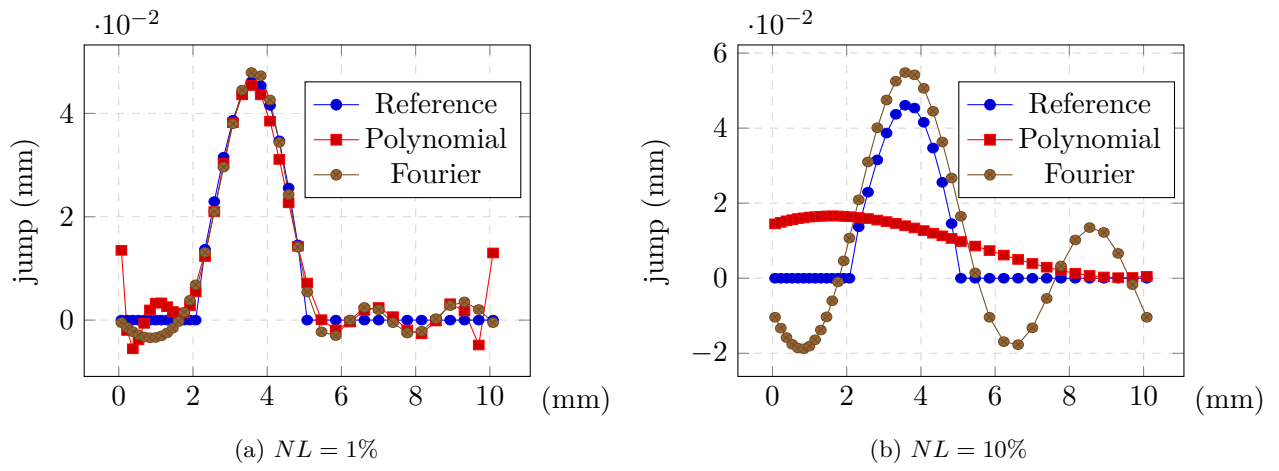


Figure 8: Identification of $\llbracket u_r \rrbracket \cdot \underline{n}_{II}$ in ω for thicknesses $h = 2$ mm with noise

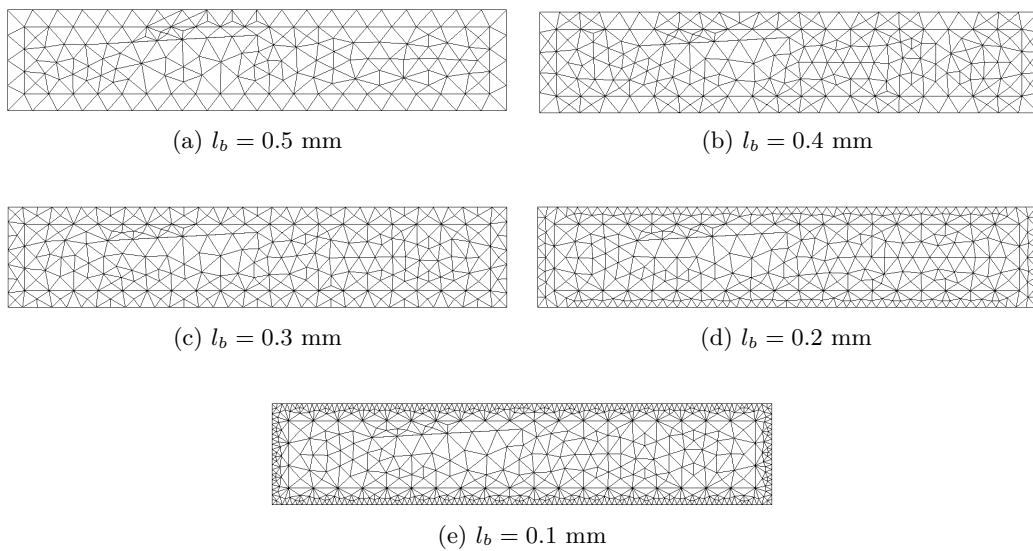


Figure 9: Different meshes used for the refinement study

5.2 3D cracks

This numerical experiment focuses on the detection of cracks on an unknown internal surface inside a three-dimensional elastic body.

The cracked body consists of a cuboid with dimensions $10 \times 7 \times h$ filled with homogeneous isotropic elastic material ($E = 210,000$ MPa, $\nu = .3$). It contains two elliptic cracks: S_1 with main axes $a_1 = 2$ and $b_1 = 1$ parallel to the x and y directions, and S_2 with main axes $a_2 = 1.5$ and $b_2 = 2.5$ and making an angle of $\frac{\pi}{15}$ around the y axis. The crack S_1 has its center at $(4, 2, \frac{h}{2})$ and S_2 is centered at $(4, 7, \frac{h}{2})$. This geometry is illustrated on figure 10.

Each of the two experiments consists in an uniform traction load, parallel to an axis and applied on two faces. The first one is a traction along \underline{e}_z and the second one is a traction along \underline{e}_x .

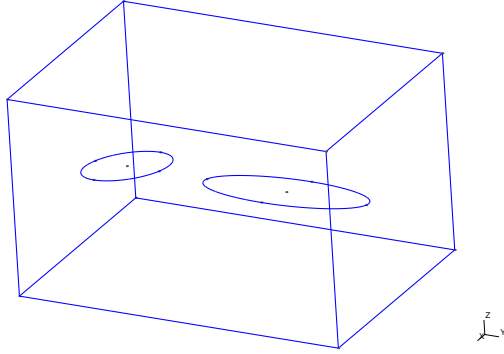


Figure 10: Geometry of the studied cracked domain

5.2.1 Comparison between polynomial and Fourier reconstruction

We consider first the identification of the crack's plane parameters for noise free data. The first criterion to evaluate the quality of this identification is the scalar product p_n between the real normal of the crack plane and the identified one. This scalar product must be close to 1. The second criterion is the distance d_π between the identified plane and the center of the big ellipse (at $(4, 7, \frac{h}{2})$), that must be as small as possible. The results are given in Table 3. They show that in the absence of any noise, the estimation of the crack's plane is very accurate.

Height	$H = 2$	$H = 4$	$H = 6$	$H = 10$
p_n	1.0000	1.0000	1.0000	1.0000
d_π (mm)	$8.1556 \cdot 10^{-6}$	$1.0724 \cdot 10^{-5}$	$4.8479 \cdot 10^{-6}$	$3.6787 \cdot 10^{-6}$

Table 3: Identification of the parameters of the crack plane in absence of noise

We consider then the reconstruction of the displacement jump for the Fourier and polynomial method (see Figures 11, 12, 13, 14 and Table 4). The error that is studied is defined as the L^2 norm on ω of the difference between the reconstructed gap and the reference gap extracted from the direct finite element computation. It is noticeable that the polynomial approach gives fairly better results than the Fourier approach for thick domains.

Height (mm)	$H = 2$	$H = 4$	$H = 6$	$H = 10$
Order of Fourier test-functions	3	1	1	-
L^2 Error for Fourier approach	0.37	1.6	5.5	-
Order of polynomial test-functions	15	15	11	10
L^2 Error for polynomial approach	0.085	0.12	0.13	0.19

Table 4: Error and number of modes for the noise free case

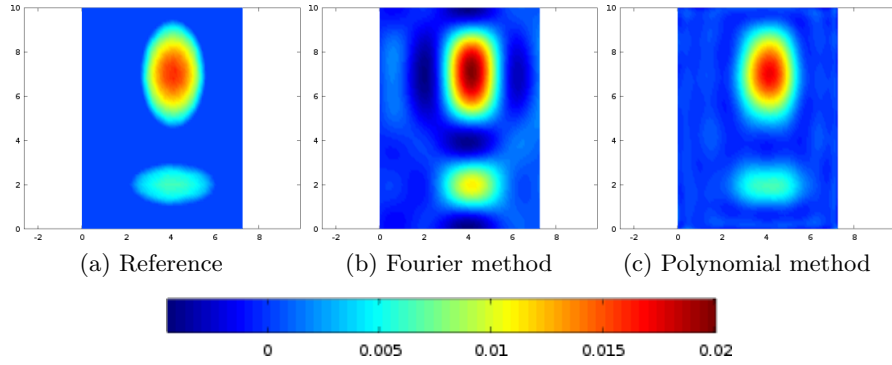


Figure 11: Reference and reconstruction of the gap for $h = 2$ mm

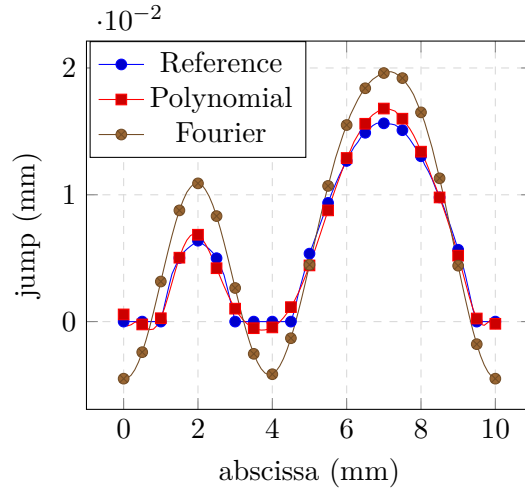


Figure 12: Reference and reconstruction of the gap on the line $x = 4$ mm with $h = 2$ mm

5.2.2 Study of different crack geometries

A few different geometries were identified on a 2 mm thick domain without noise. The results are presented on Figures 15 and 16, they show that while the position and size of the crack is always fairly identifiable, its exact shape may be harder to recover.

The difference between a rectangular, elliptical or rhombus crack is hard to make from the reconstructed displacement gap in the plane. What is more, Figure 16 shows that for a complex and non-convex shape, only the most bulky part of the crack is reconstructed.

5.2.3 Robustness in presence of noise and comparison between regularization processes

In this part, a Gaussian noise is added to the measurements. The noise level is denoted by NL . The goal is to compare the results given by the different regularization schemes presented in Part 4. Table 5 contains the quantitative results for the identification of the crack's plane (scalar product p_n between identified and reference normal and distance d_π between the center of the crack and the identified plane).

	$NL = 0 \%$	$NL = 2 \%$	$NL = 10 \%$
p_n	1.0000	0.9997	.9998
d_π (mm)	$8.1556 \cdot 10^{-6}$	0.1701	0.3836

Table 5: Identification of the crack plane

On Figure 17, the displacement gap cartographies, L^2 errors and optimal regularization parameters for different noise levels and different regularization schemes. The parameters are the maximal order of

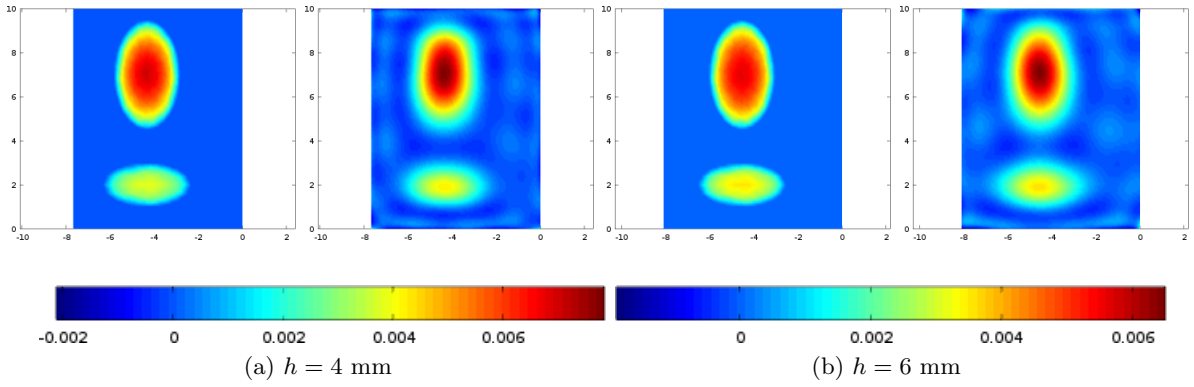


Figure 13: Reference compared to the polynomial identification

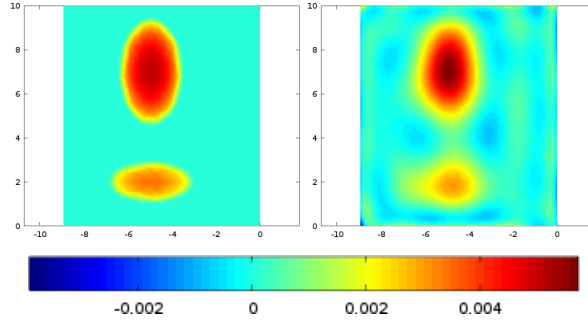


Figure 14: Reference compared to the polynomial identification for $h = 10$ mm

polynomials for the truncation K , the total number of polynomials N and the Tikhonov regularization parameter μ . Those parameters have been tuned by hand in order to obtain the better looking solution. Unfortunately, the parameter N has to be tuned as keeping it at the maximal value results in over-oscillating solutions. All the solutions on the line $x = -4$ mm in Π are compared on Figure 18.

We observe that the gradient-penalizing regularization methods give better identification results. The Tikhonov method is superior to the *a posteriori* method as it results in less oscillations in the cartographies and in lower errors. Finally, the methods based on the total variation do not seem to lead to significant improvement of the reconstruction compared to quadratic regularization, while being much more expensive in terms of computational resources and implementation effort.

5.2.4 Experiment in case of non-planar crack

All the methods presented above rely on the assumption that the crack is planar. In this subsection, we evaluate numerically how the method behaves in the case of a slightly non-planar crack. The crack is constituted of two semi-ellipses with main axes $a = 2.5$ and $b = 1.5$ mm, that are not perfectly coplanar. The angle between the semi-ellipses is $\frac{\pi}{10}$.

The identification procedure results in a planar crack whose normal is not far from the bisector between the normal vector of the semi-ellipses ($p_n = 0.9869$), and which is only distant of 0.1885 mm from the center of the common segment of the semi-ellipses. This distance is quite small compared to the size of the ellipses.

The result of the reconstruction of the displacement jump, presented on figure 19, shows that while the non-respect of the planarity hypothesis induces a perturbation of the identification, the shape and localization of the crack are still fairly well reconstructed. A similar result was obtained in [8] for the Helmholtz equation with the Fourier approximation.

5.2.5 Summary of the numerical tests

- The Fourier method gives fairly stable solutions for thin domains, but is not suited to thick ones.
- The polynomial method gives accurate identification results for small noise level and relatively

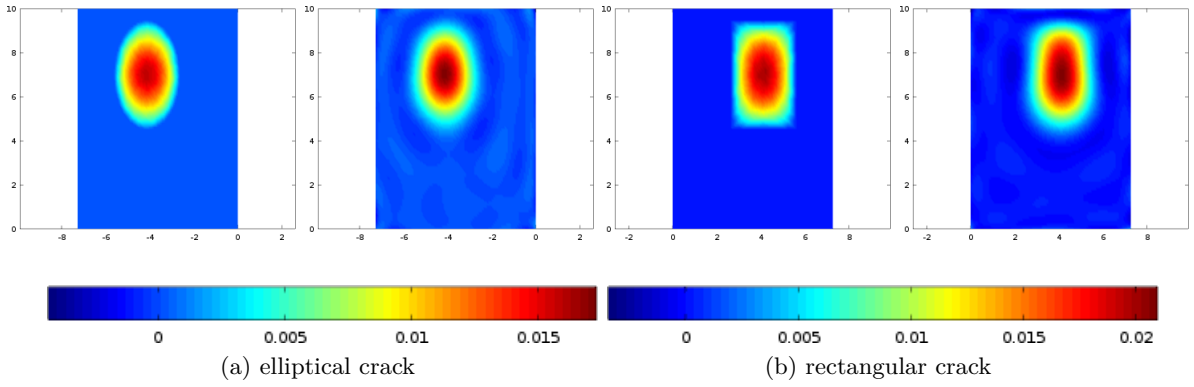


Figure 15: Identification of different shapes. $h = 2$ mm

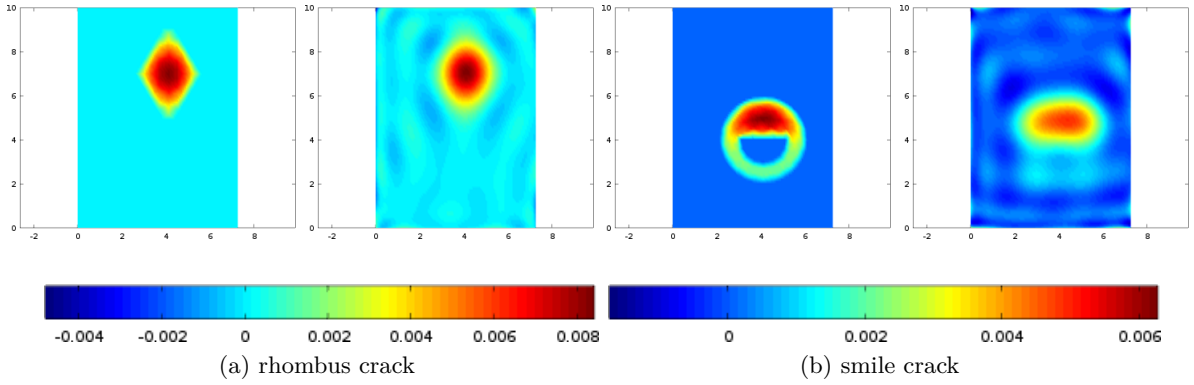


Figure 16: Identification of different shapes. $h = 2$ mm

thick domains, however for noise level around 10%, or in case of really thick domains, the identification quality deteriorates (see figure 14 and Figure 17).

- In general, exceeding an order 15 for the polynomial approximation does not ameliorate the solution.
- The use of a regularization strategy that penalizes the gradient gives slightly better results than the truncation of the approximation basis.
- The total variation and quadratic regularization terms give results of similar quality. As the latter is way easier to implement and less CPU expensive, it should probably be preferred.

Conclusion and perspectives

This paper provides an implementation, in the 3D and 2D plane stress cases, of the crack identification formulas proposed in [4]. Numerical and analytical results show that, the initially proposed Fourier reconstruction is mostly adapted to thin domains. We propose a new polynomial reconstruction which appears to be more stable for thick domain. Moreover, we propose regularization schemes based on the truncation of the reconstruction basis and on the minimization of the gradients of the displacement jump. The Tikhonov regularization method gives slightly better results than the raw truncation of the approximation basis, this method is more complex to implement and to tune properly.

As the construction of test-functions respecting the local equilibrium $\text{div}(\underline{\sigma}(v)) = \underline{0}$ and permitting the reconstruction of the jump field in the plane is laborious, the next step of this work is to replace the Galerkin projection by a Petrov-Galerkin approximation, permitting to separate the role of test-functions and approximation functions.

Reference						
Noise Level	$NL = 2 \%$			$NL = 10 \%$		
	Displacement jump	L^2 error	Regularization parameters	Displacement jump	L^2 error	Regularization parameters
Truncation		0.303	$K = 9$		0.612	$K = 5$
<i>a posteriori</i> quadratic		0.300	$K = 9$ $N = 12$		0.563	$K = 5$ $N = 10$
<i>a posteriori</i> TV		0.301	$K = 9$ $N = 12$		0.559	$K = 5$ $N = 10$
Tikhonov quadratic		0.254	$N = 12$ $\mu = .1$		0.471	$N = 7$ $\mu = .1$
Tikhonov TV		0.249	$N = 12$ $\mu = .001$		0.479	$N = 7$ $\mu = .001$

Figure 17: Displacement gap identification for noisy data and regularization

A A posteriori total variation minimization algorithm

We want to solve the non-quadratic minimization problem (34). As no polynomial expression can be found for $|\mathbf{D}_N \mathbf{v}|$, it was chosen to compute its integral by approximating it by a stepwise constant function on a rectangular mesh, with M rectangles. The gradient operator \mathbf{D}_N can then be discretized into an operator denoted by \mathbf{G} that gives the value of the gradient at the barycenter of each of the M rectangles from the polynomial coefficients and has size $M \times N$. The system (38) results from this. $|\bullet|$ is the componentwise absolute value and S_j is the area of the j th rectangle.

$$(\hat{u}_i)_{1 \leq i \leq N} = \arg \min_{(v_i = u_i)_{1 \leq i \leq K}} \sum_{j=1}^M S_j |\mathbf{G} \mathbf{v}|_j \quad (38)$$

We introduce the projector \mathbf{I}_\perp on the K first components, such that $\mathbf{I}_\perp \mathbf{v} = \mathbf{I}_\perp \mathbf{u}$ is equivalent to $(v_i = u_i)_{1 \leq i \leq K}$. We also introduce the vector \mathbf{I}_Σ which corresponds to the weighted sum over all components $1 \leq j \leq M$. The minimization problem hence becomes:

$$\min_{\mathbf{I}_\perp \mathbf{v} = \mathbf{I}_\perp \mathbf{u}} \mathbf{I}_\Sigma^T |\mathbf{G} \mathbf{v}| \quad (39)$$

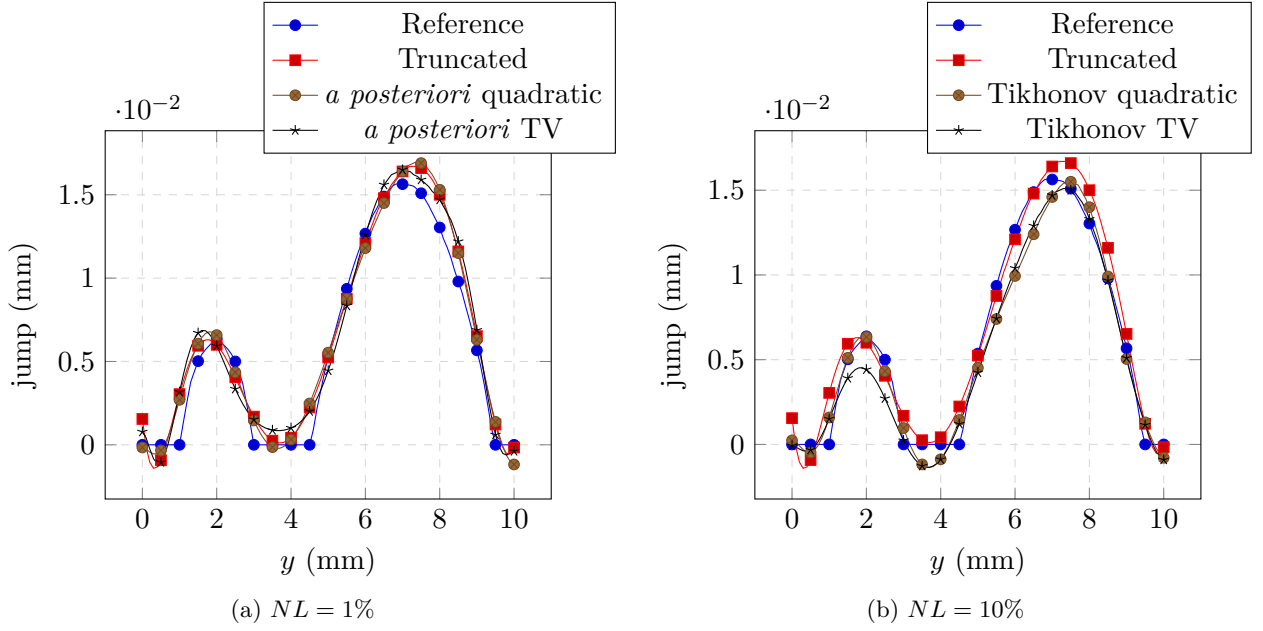


Figure 18: Reference and solution with different regularization techniques ($h = 2$ mm) on the line $x = -4$ mm

In order to cast this equation into a classical linear programming problem, we introduce the vector \mathbf{x} meant to be equal to $|\mathbf{G}\mathbf{v}|$. We have $-\mathbf{x} \leq \mathbf{G}\mathbf{v} \leq \mathbf{x}$ and we can search for (\mathbf{v}, \mathbf{x}) solutions to:

$$\begin{aligned} & \min_{\mathbf{v}, \mathbf{x}} \quad (0 \quad \mathbf{I}_{\Sigma}^T) \begin{pmatrix} \mathbf{v} \\ \mathbf{x} \end{pmatrix} \\ & \mathbf{I}_{\perp} \mathbf{v} = \mathbf{I}_{\perp} \mathbf{u} \\ & \begin{pmatrix} \mathbf{G} & -\mathbf{I}_d \\ -\mathbf{G} & -\mathbf{I}_d \end{pmatrix} \begin{pmatrix} \mathbf{v} \\ \mathbf{x} \end{pmatrix} \leq \begin{pmatrix} 0 \\ 0 \end{pmatrix} \end{aligned} \quad (40)$$

Under this form, we can use functions of the *glpk* [18] library, which is interfaced with Octave.

B Dual method for the minimization of a total variation regularized functional

We want to solve the problem (36). Using the notations of previous appendix, the system reads:

$$\mathbf{u}_{N,1} = \arg \min_{\mathbf{v}} \frac{1}{2} \mathbf{v}^T \mathbf{B}_N \mathbf{v} - \mathbf{v}^T \mathbf{b}_N + \mu \mathbf{I}_{\Sigma} |\mathbf{G}\mathbf{v}| \quad (41)$$

The method is adapted from an other approach coming from the image processing community [10]. It consists in solving a dual problem. As $\mathbf{I}_{\Sigma} \geq 0$, we can introduce a dual vector \mathbf{w} to get:

$$\mathbf{I}_{\Sigma}^T |\mathbf{G}\mathbf{v}| = \max_{|\mathbf{w}| \leq \mathbf{I}_{\Sigma}} \mathbf{w}^T \mathbf{G}\mathbf{v} \quad (42)$$

Consequently, the minimization problem (41) becomes :

$$\min_{\mathbf{v}} \max_{|\mathbf{w}| \leq \mathbf{I}_{\Sigma}} \frac{1}{2} \mathbf{v}^T \mathbf{B}_N \mathbf{v} - \mathbf{v}^T \mathbf{b}_N + \mu \mathbf{w}^T \mathbf{G}\mathbf{v} \quad (43)$$

As the objective function is convex in \mathbf{v} and concave in \mathbf{w} , and as $|\mathbf{w}| \leq \mathbf{I}_{\Sigma}$ is a bounded domain, the previous optimization problem is equivalent to problem (44).

$$\max_{|\mathbf{w}| \leq \mathbf{I}_{\Sigma}} \min_{\mathbf{v}} \frac{1}{2} \mathbf{v}^T \mathbf{B}_N \mathbf{v} - \mathbf{v}^T \mathbf{b}_N + \mu \mathbf{w}^T \mathbf{G}\mathbf{v} \quad (44)$$

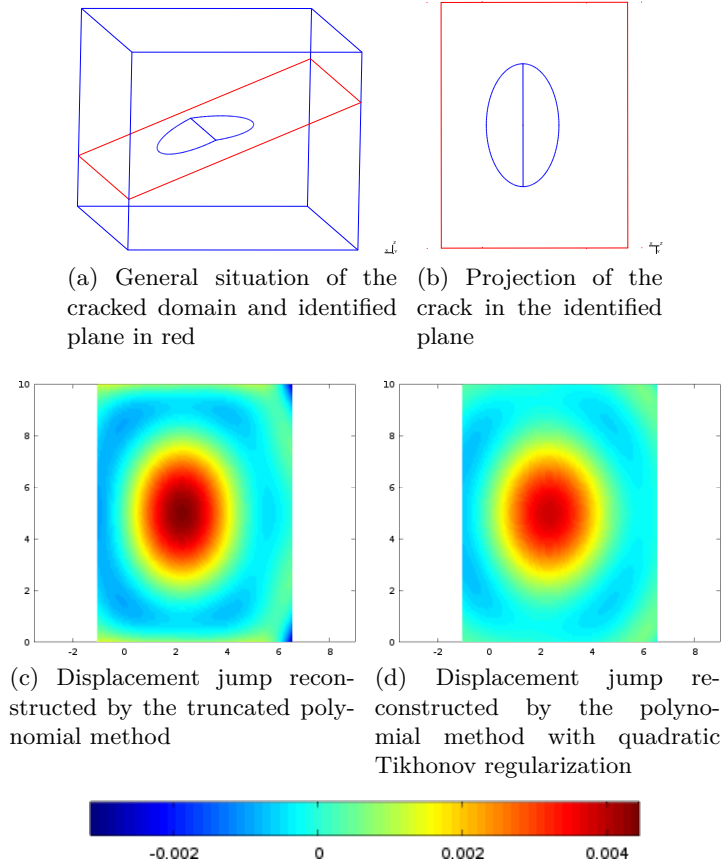


Figure 19: Identification of a non-planar crack in a 6 mm thick domain

The minimum can be found for \mathbf{v} :

$$\mathbf{v} = \mathbf{B}_N^{-1}(\mathbf{b}_N - \mu \mathbf{G}^T \mathbf{w}) \quad (45)$$

Thus, the problem can be simplified by replacing \mathbf{v} by its expression and changing max into min :

$$\min_{|\mathbf{w}| \leq \mathbf{I}_\Sigma} \frac{1}{2} \mathbf{w}^T (\mathbf{G} \mathbf{B}_N^{-1} \mathbf{G}^T) \mathbf{w} - \mathbf{w}^T \left(\mathbf{G} \mathbf{B}_N^{-1} \frac{\mathbf{b}_N}{\mu} \right) \quad (46)$$

Note that as \mathbf{G} is a rectangular derivation operator, it is rank-deficient, but $\mathbf{G} \mathbf{B}_N^{-1} \frac{\mathbf{b}_N}{\mu}$ is orthogonal to the kernel of $\mathbf{G} \mathbf{B}_N^{-1} \mathbf{G}^T$. Because of this kernel, the problem (46) cannot be solved via an Uzawa method. The status method is likely to fail because of the high number of constraints and the ill-conditioning of the operators. For that reason, an alternating directions algorithm was chosen, inspired from [17]. We search for a couple (\mathbf{u}, \mathbf{f}) that belongs to both of the spaces \mathcal{L} and \mathcal{N} defined below:

$$(\mathbf{u}, \mathbf{f}) \in \mathcal{L} \Leftrightarrow \left\{ \mathbf{G} \mathbf{B}_N^{-1} \mathbf{G}^T \mathbf{u} = \mathbf{G} \mathbf{B}_N^{-1} \frac{\mathbf{b}_N}{\mu} + \mathbf{f} \right\} \quad (47)$$

$$(\mathbf{u}, \mathbf{f}) \in \mathcal{N} \Leftrightarrow \{ \forall \text{dof } i, |u_i| \leq \mathbf{I}_{\Sigma, i}, \text{sign}(u_i) f_i \leq 0, f_i(u_i - \mathbf{I}_{\Sigma, i}) = 0 \text{ or } f_i(u_i + \mathbf{I}_{\Sigma, i}) = 0 \}$$

If $(\mathbf{u}, \mathbf{f}) \in \mathcal{L} \cap \mathcal{N}$ then \mathbf{u} is the minimizer of (46).

The algorithm consists in finding alternatively solutions in \mathcal{N} and in \mathcal{L} respecting respectively:

$$\begin{aligned} (\mathbf{u}_n, \mathbf{f}_n) &\in \mathcal{L} \quad \text{with} \quad \mathbf{f}_n = \mathbf{f}_{n-1/2} + k(\mathbf{u}_n - \mathbf{u}_{n-1/2}) \\ (\mathbf{u}_{n+1/2}, \mathbf{f}_{n+1/2}) &\in \mathcal{N} \quad \text{with} \quad \mathbf{f}_{n+1/2} = \mathbf{f}_n + k(\mathbf{u}_{n+1/2} - \mathbf{u}_n) \end{aligned} \quad (48)$$

where k is a parameter of the method that should be chosen close to the spectral radius of $\mathbf{G} \mathbf{B}_N^{-1} \mathbf{G}^T$

Finding a couple in \mathcal{N} is a global linear problem, while finding a couple in \mathcal{L} results in a nonlinear problem, that can be solved independently on each degree of freedom i . Finally, we choose to relax this method at each step with a relaxation parameter of value $1/2$.

References

- [1] S. Andrieux and T. Baranger. Emerging crack front identification from tangential surface displacements. *Comptes Rendus Mecanique*, 340:565–574, 2012.
- [2] S. Andrieux and A. Ben Abda. The reciprocity gap: a general concept for flaws identification problems. *Mechanics research communications*, 20(5):415–420, 1993.
- [3] S. Andrieux, A. Ben Abda, and H. D. Bui. Sur l’identification de fissures planes via le concept d’écart à la réciprocité en élasticité. *Comptes Rendus de l’Académie des Sciences-Series I-Mathematics*, 324(12):1431–1438, 1997.
- [4] S. Andrieux, A. Ben Abda, and H. D. Bui. Reciprocity principle and crack identification. *Inverse problems*, 15(1):59, 1999.
- [5] S. Andrieux, A. Ben Abda, and M. Jaoua. On the emerging plane crack problem. *INRIA J.*, 3012, 1996.
- [6] T. Bannour, A. Ben Abda, and M. Jaoua. A semi-explicit algorithm for the reconstruction of 3D planar cracks. *Inverse Problems*, 13(4):899, 1997.
- [7] A. Ben Abda, H. Ben Ameer, and M. Jaoua. Identification of 2D cracks by elastic boundary measurements. *Inverse Problems*, 15(1):67, 1999.
- [8] A. Ben Abda, F. Delbary, and H. Haddar. On the use of the reciprocity-gap functional in inverse scattering from planar cracks. *Mathematical Models and Methods in Applied Sciences*, 15(10):1553–1574, 2005.
- [9] K. Bryan, F. R. Osborne III, and M. e Vellela. Reconstruction of cracks with unknown transmission condition from boundary data. *Inverse Problems*, 21(1):21, 2004.
- [10] T. F. Chan, G. H. Golub, and P. Mulet. A nonlinear primal-dual method for total variation-based image restoration. *SIAM journal on scientific computing*, 20(6):1964–1977, 1999.
- [11] T. F. Chan, H. M. Zhou, and R. H. Chan. *Continuation method for total variation denoising problems*. Department of Mathematics, University of California, Los Angeles, 1995.
- [12] A. Elcrat, V. Isakov, and A. Necoloin. On finding a surface crack from boundary measurements. *Inverse Problems*, 11:343–351, 2001.
- [13] M. Eller. Identification of cracks in three dimensional bodies by many boundary measurements. *Inverse Problems*, 12:527–556, 2005.
- [14] A. Friedman and M. Vogelius. Determining cracks by boundary measurements. *Indiana Univ. Math. J.*, 106:527–559, 2000.
- [15] P. C. Hansen. Analysis of discrete ill-posed problems by means of the l-curve. *SIAM review*, 34(4):561–580, 1992.
- [16] M. L. Kadri, J. B. Abdallah, and T. N. Baranger. Identification of internal cracks in a three-dimensional solid body via Steklov–Poincaré approaches. *Comptes Rendus Mécanique*, 339(10):674–681, 2011.
- [17] P. Ladevèze. *Nonlinear computational structural mechanics: new approaches and non-incremental methods of calculation*. Springer, 1998.
- [18] A. Makhorin. GLPK (GNU linear programming kit). <http://www.gnu.org/s/glpk/glpk.html>, 2008.
- [19] V. A. Morozov. The error principle in the solution of operational equations by the regularization method. *Zhurnal Vychislitel’noi Matematiki i Matematicheskoi Fiziki*, 8(2):295–309, 1968.

- [20] E. Shifrin and P. Shushpannikov. Identification of small well-separated defects in an isotropic elastic body using boundary measurements. *International Journal of Solids and Structures*, 50(22):3707–3716, 2013.
- [21] P. Steinhorst and B. Kaltenbacher. Application of the reciprocity principle for the determination of planar cracks in piezoelectric material. In *Advanced Finite Element Methods and Applications*, pages 325–353. Springer, 2013.
- [22] P. Steinhorst and A. Sändig. Reciprocity principle for the detection of planar cracks in anisotropic elastic material. *Inverse Problems*, 28(8):085010, 2012.